Harvesting wind energy to detect weak signals using mechanical stochastic resonance

Barbara J. Breen,* Jillian G. Rix, Samuel J. Ross, and Yue Yu (俞越)
Physics Department, Grinnell College, Grinnell, Iowa 50112, USA

John F. Lindner, Nathan Mathewson, Elliot R. Wainwright, and Ian Wilson
Physics Department, The College of Wooster, Wooster, Ohio 44691 USA
(Received 6 September 2016; published 7 December 2016)

Wind is free and ubiquitous and can be harnessed in multiple ways. We demonstrate mechanical stochastic resonance in a tabletop experiment in which wind energy is harvested to amplify weak periodic signals detected via the movement of an inverted pendulum. Unlike earlier mechanical stochastic resonance experiments, where noise was added via electrically driven vibrations, our broad-spectrum noise source is a single flapping flag. The regime of the experiment is readily accessible, with wind speeds ∼20 m/s and signal frequencies ∼1 Hz. We readily obtain signal-to-noise ratios on the order of 10 dB.

DOI: 10.1103/PhysRevE.94.062205

I. INTRODUCTION

Energy harvesting is an exciting research area in which attempts are made to extract clean energy from ambient sources to power small electronic devices [1–3]. Energy harvester energy sources are free. A classic example is a crystal radio receiver powered by the received radio waves. Especially interesting is the potential for *nonlinear* energy harvesting [4,5]. While linear energy harvesters typically tune their resonant frequencies to narrow spectral regions, nonlinear nonresonant oscillators can have much wider spectral responses.

Stochastic resonance is a well-studied phenomenon where ambient noise amplifies weak signals in nonlinear systems [6,7]. In bistable or threshold systems, broadband noise can boost faint signals, too weak for a sensor to detect otherwise, from subthreshold to superthreshold. Stochastic resonance has modeled a wide range of phenomena, from ice ages to hair cells [8–11]. Stochastic resonance has even been used for energy harvesting in bistable vibrating systems: Zheng *et al.* recently demonstrated stochastic resonance in a mechanical system of a cantilevered beam with an electrical vibrator as a noise source [12,13].

Here we describe stochastic resonance in a simple mechanical system with an aeromechanical noise source. We achieved stochastic resonance by harvesting the noisy energy of a flapping flag to amplify weak periodic signals delivered to a bistable inverted pendulum. We find that the flapping flag can be an excellent broadband noise source and realize signal-to-noise ratios from 10 to 20 dB for moderate wind speeds of 20–25 m/s.

In this article, Sec. II reviews theories of stochastic resonance and our bistable system. Section III describes our apparatus construction. Section IV details our experimental protocol. Section V analyzes our results. Section VI offers a summary, applications, and future work.

II. THEORY

A. Stochastic resonance

Model a damped inverted pendulum at an angle θ by

$$I\ddot{\theta} = -\gamma\dot{\theta} - V'[\theta] + \tau_D \sin[2\pi f_D t] + \tau_N \xi[t], \qquad (1)$$

where I is the rotational inertia, γ is the viscosity, τ_D is the drive torque, f_D is the drive frequency, τ_N is the root-mean-square noise torque, and $\xi[t]$ is a random process with zero mean and unit variance. Overdots indicate time derivatives, and the prime indicates derivative with respect to the argument. The bistable potential $V[\theta]$ has two wells separated by a barrier. If the barrier height between the wells is ΔE and the vibrational noise has a variance σ^2 and correlation time τ, the probability of transition between the wells is proportional to the Kramers rate [14], whose leading behavior is given by the Arrhenius or Boltzmann factor

$$\mathcal{P} \sim f_K \sim e^{-\Delta E/kT}, \qquad (2)$$

where the effective temperature $kT = \sigma^2\tau/\gamma$.

In mechanical resonance, the periodic drive frequency equals a system's natural frequency $f_D = f_0$. In stochastic resonance, the drive frequency is half the Kramers rate,

$$f_D = \frac{f_K}{2}, \qquad (3)$$

so that on average the transitions between wells occur twice each drive period and $T_D = 2T_K$ [15].

In practice, Fourier techniques reveal the statistical correlation between a weak periodic signal and noise in a bistable system. The power spectral density, or spectrum S, is proportional to the absolute square of the Fourier transform of the time series. The weak periodic drive embedded in the noise produces a narrow spectral peak at the drive frequency f_D against a broad noise background. The signal-to-noise ratio

$$R = \frac{S_\wedge - N}{N} = \frac{S_\wedge}{N} - 1 \geqslant 0, \qquad (4)$$

where $S_\wedge = S[f_D]$ is the spectrum at the drive frequency and N is the background noise about the drive frequency. This definition ensures $R = 0$ in the absence of the drive. The signature of stochastic resonance is a local maximum of R at a nonzero value of noise.

B. Inverted pendulum spring

Our bistable element is an inverted pendulum of length ℓ rotating back and forth between two stops. We attach a spring of stiffness k and equilibrium length ℓ_0 to the pendulum bob

*Corresponding author: breenbar@grinnell.edu

of mass m. The spring is anchored a distance h directly below the pivot axle. If the angle $\theta = 0$ defines the upward vertical position of the pendulum, then the torque between the stops is

$$\tau_\theta = mg\ell \sin\theta + kh\ell\left(1 - \frac{\ell_0}{\sqrt{h^2 + 2h\ell\cos\theta + \ell^2}}\right)\sin\theta, \tag{5}$$

where g is the gravitational acceleration [16]. The corresponding potential energy

$$\begin{aligned} V &= -\int_0^\theta \tau_\theta d\theta \\ &= -(mg + kh)\ell(1 - \cos\theta) \\ &\quad + k\ell_0\left(h + \ell - \sqrt{h^2 + 2h\ell\cos\theta + \ell^2}\right) \end{aligned} \tag{6}$$

has the power-series expansion

$$V = -\tfrac{1}{2}c_k\theta^2 + O[\theta^4], \tag{7}$$

where

$$c_k = kh\ell\frac{h + \ell - \ell_0}{h + \ell} + mg\ell. \tag{8}$$

For stretched springs $\ell > \ell_0$, and so $c_k > c_0 = mg\ell$. Thus, a stretched spring increases the curvature of the potential about $\theta = 0$, ensuring unstable equilibrium even in the presence of residual friction. (Alternately, a pair of springs on either side of the pivot can replace the stops to create a classic smooth bistable potential with an unstable central maximum surrounded by two stable minima.)

III. APPARATUS

The experimental apparatus consists of three subsystems: a noise source, a drive signal, and a bistable inverted pendulum, as shown in Fig. 1. The noise source is a wind-blown flag. The flag is oriented horizontally and the wind is from a jet fan oriented vertically. A string attached to the free end of the flag wraps sliplessly over a pulley connected to the main axle about which the pendulum pivots. A counterweight attached to the other end of the string balances the mean force of the noise.

A rotary motor coupled indirectly to the experiment provides a small-amplitude sinusoidal drive signal. A string from the driver wraps sliplessly over a pulley on an axle parallel to and below the main axle. A counterweight attached to the other end of the string stabilizes the drive signal. A second pulley on the parallel axle couples the drive to the main axle via springs attached to each end of a belt that slips back and forth over a drum on the main axle.

Varying the distance between the two axles controls the strength of this frictional coupling. Increasing the distance stretches the springs and increases the frictional torque, while decreasing the distance relaxes the springs and decreases the frictional torque. Frictional slipping allows the signal and noise to cooperate in driving the pendulum.

The bistable element consists of an inverted pendulum that rotates back and forth between two hard stops. To ensure an unstable inverted equilibrium in the presence of friction, a spring is attached from the pendulum bob to below the pivot.

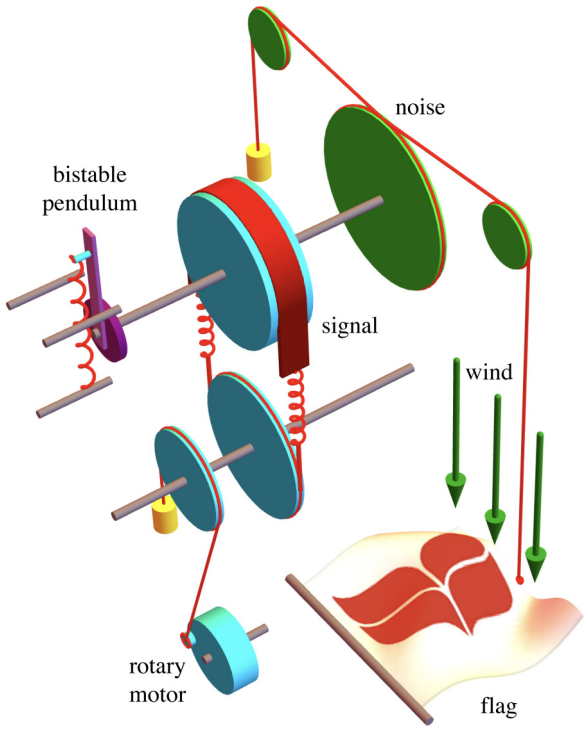

FIG. 1. Schematic of the mechanical stochastic resonance apparatus. At lower right, a wind-blown flapping flag delivers noise to the main axle via a slipless pulley. At lower left, a rotary motor delivers a subthreshold sinusoidal signal to the main axle indirectly via a tensioned slipping belt. At upper left, a bistable inverted pendulum rotates back and forth between two stops.

IV. EXPERIMENT

As part of the initial calibration of the apparatus, a string fastened to the end of the flag in the wind stream connects to a force sensor and records the mean and standard deviation of the force as a function of wind speed. The root-mean-square flag force increases quadratically with wind speed. We use the mean force values to select counterweights that balance the noise coming from the flag. We adjust the counterweight to center the pendulum motion for each wind speed, providing approximately zero-mean torque to the bistable pendulum. We initialize the flag in its neutral horizontal position, while the pendulum rests at its neutral $\theta = 0$ unstable equilibrium. The string connecting the flag to the pendulum axle always starts at the same length, sufficient to allow equal up and down motion of the flag.

The drive subsystem includes two pulleys on an axle parallel to and below the main axle, as in Fig. 1. The rotary motor is connected to the first of the two lower pulleys by a string with a counterweight on the other end. If the counterweight is too light, the string will slip during the upstroke but not during the downstroke. To ensure symmetry of the periodic drive, we use a 150 g counterweight. A photogate separately monitors the $f_D = 1.0$ Hz drive frequency. The second pulley transfers this balanced drive signal to the main axle via a string-spring-belt loop. We adjust the distance between the two axles such that the pendulum oscillates from 10° to 30° on one side of zero or the other, so that in the absence of noise the drive is insufficient

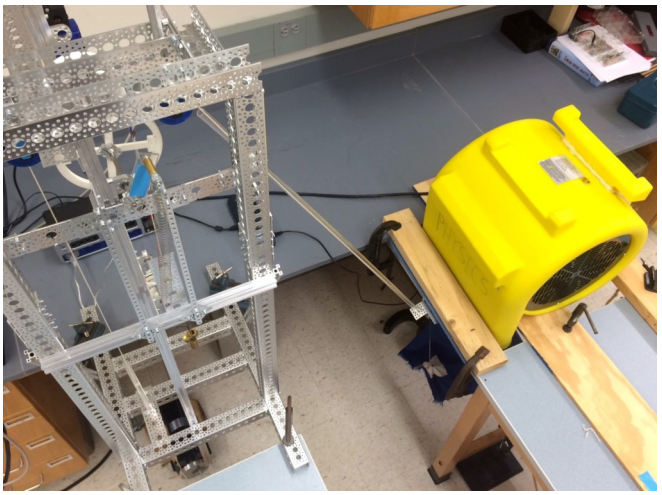

FIG. 2. Apparatus photograph. At right, the jet fan blows downward on the horizontal flag. At left, the inverted (blue) pendulum tops the tower. At center, a string passing through the acrylic tube couples the motion of the flag to the rotation of the pendulum. At bottom left, a rotary motor provides the drive signal.

to cause the pendulum to rotate through zero. This ensures a subthreshold signal that can be promoted to a superthreshold signal via the addition of noise.

To create a robust bistable subsystem, we adjust the mass of the pendulum bob $m = 25$ g, the pendulum spring stiffness $k = 3.3$ N/m, equilibrium length $\ell_0 = 6.1$ cm, and maximum (upright) stretch $\ell_m = 31$ cm. We adjust the location of the stops, as in the upper left of Fig. 2, to allow the pendulum to oscillate up to 30° in either direction.

A variable autotransformer Variac controls the voltage to the fan to provide a continuous range of wind speeds from 15 to 25 m/s, which are monitored by an anemometer. In successive 30-min recordings, we swap Variacs to guard against overheating. We record the motion of the pendulum with a rotary motion sensor. To enable statistical analysis, we typically record six 30-min time series for each wind speed. If necessary, we adjust the Variac while recording to maintain a constant wind speed for each time series.

V. ANALYSIS

A typical pendulum time series $\theta[t]$ consists of intrawell and interwell motion, as in the continuous (black) trace of Fig. 3. The stops at $\pm 30^\circ = \pm 0.52$ rad demarcate the potential minima. We remove the intrawell motion by filtering the time series with a hysteresis to extract only barrier crossings, as in the discrete (red) trace $\theta_F[t]$. When the angle (black trace) rises above a positive threshold, we pin the filtered angle (red trace) to a positive value, and when the angle falls below a negative threshold, we pin the filtered angle to a negative value.

We Fourier transform the filtered time series $\theta_F[t]$ to get $\tilde{\theta}_F[f]$. Figure 4 shows typical power spectral densities (grays) $S[f] = |\tilde{\theta}_F[f]|^2$ along with their average (red). Averaging reduces noise variation and makes the signal peak at drive frequency more distinct [17]. The inset shows the broadband nature of the noise alone.

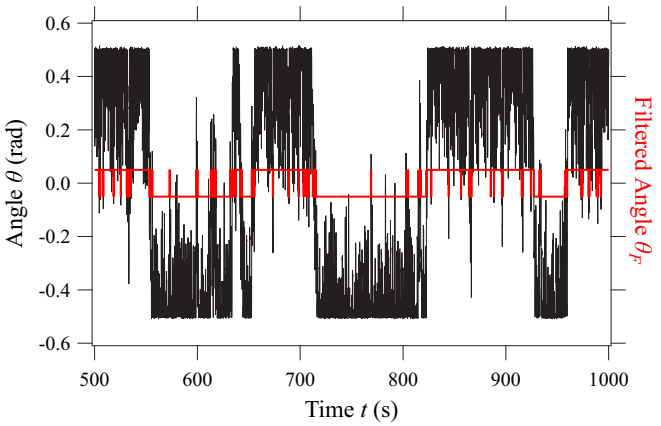

FIG. 3. Angle θ vs time t for a typical time series with wind speed $v_w = 19$ m/s. Continuous unfiltered (black) data exhibit both interwell and intrawell motion. Discrete filtered (red) data record only interwell motion.

To compute the Eq. (4) signal-to-noise ratio R, we find the area in square radians of the peak at the drive frequency and divide it by the corresponding area of the background noise (found by linear interpolation of the noise about the signal, but not containing it).

For Fig. 5, we calculate R for each times series and average the results for each wind speed. The signal-to-noise ratio has a local maximum near $v_w = 23$ m/s. Uncertainty box sizes are plus or minus one standard deviation. When we average the spectra first and then find one R per wind speed, we obtain similar results. The stochastic resonance is robust with respect to the details of our analysis. The top inset plots the signal-to-noise ratio in decibels versus the variance of the flag force noise, a classic stochastic resonance curve. The bottom inset plots the filtered time series near the stochastic resonance, where an average of two transitions per forcing period $T_D = 1/f_D = 1$ s agrees with the Eq. (3) Kramers condition, with the fluctuations of the wind-blown flag playing the role of an effective temperature.

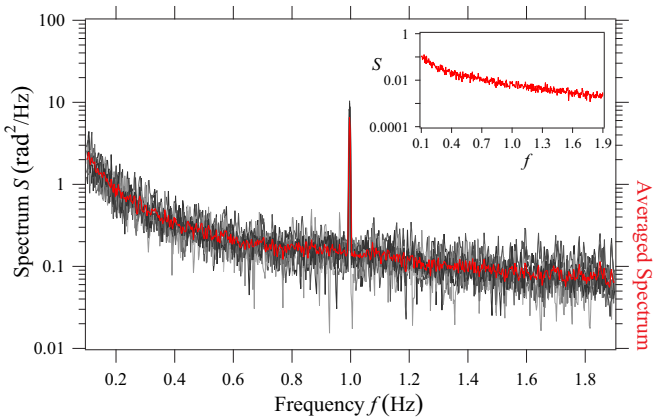

FIG. 4. Power spectral density or spectrum S vs frequency f with wind speed $v_w = 23$ m/s. The (red) average spectrum overlays the (gray) spectra from individual time series. Averaging reduces noise variation and makes more distinct the signal peak at drive frequency $f_D = 1.0$ Hz. Inset: spectrum S (rad^2/Hz) vs frequency f (Hz) for noise only.

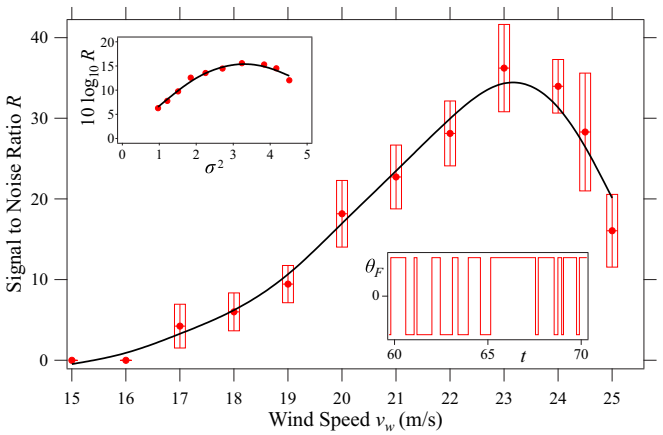

FIG. 5. Signal-to-noise ratio R vs wind speed v_w for the filtered time series. A smoothing spline connects uncertainty boxes. Stochastic resonance occurs near wind speed $v_w = 23$ m/s where the noise cooperates with the weak signal to maximize the signal-to-noise ratio. Insets: at top, ratio R (dB) vs noise variance σ^2 (N^2); at bottom, filtered angle θ_F vs time t (s) near resonance.

VI. CONCLUSIONS

Modern windmills use turbines to convert the kinetic energy of moving air into electricity. But even the noisy fluttering of a flag in a breeze can amplify periodic signals using stochastic resonance. In this article, we demonstrate mechanical stochastic resonance in an elegant tabletop experiment in which wind energy is harvested to amplify weak periodic signals detected via the movement of an inverted pendulum. Moderate wind speeds can significantly amplify low-frequency signals.

In the future, we hope to build smaller wind-powered stochastic resonance experiments that operate at higher frequencies to reduce data collection times. Flapping flags can be excellent broadband noise sources, provided they do not flutter periodically [18,19], and they can power diverse stochastic systems, including spatiotemporal and noise-enhanced stochastic resonance experiments [20,21]. The ubiquity of wind and the simplicity and broad spectral response of flapping flags suggest the potential for diverse applications.

ACKNOWLEDGMENTS

This research was supported in part by a grant to Grinnell College from the Howard Hughes Medical Institute Grant Award No. 52007542 through the Precollege and Undergraduate Science Education Program. We appreciate the assistance of Yashasvi Lohia and Noah Megregian.

[1] N. Elvin and A. Erturk, *Advances in Energy Harvesting Methods* (Springer, New York, 2013).
[2] R. L. Harne and K. W. Wang, Smart Mater. Struct. **22**, 023001 (2013).
[3] S. Ulukus, A. Yener, E. Erkip, O. Simeone, M. Zorzi, P. Grover, and K. Huang, IEEE J. Sel. Areas Commun. **33**, 360 (2015).
[4] F. Cottone, H. Vocca, and L. Gammaitoni, Phys. Rev. Lett. **102**, 080601 (2009).
[5] A. Haji Hosseinloo and K. Turitsyn, Phys. Rev. Appl. **4**, 064009 (2015).
[6] K. Wiesenfeld, F. Moss, *et al.*, Nature (London) **373**, 33 (1995).
[7] L. Gammaitoni, P. Hänggi, P. Jung, and F. Marchesoni, Rev. Mod. Phys. **70**, 223 (1998).
[8] R. Benzi, A. Sutera, and A. Vulpiani, J. Phys. A **14**, L453 (1981).
[9] C. Nicolis and G. Nicolis, Tellus **33**, 225 (1981).
[10] R. Benzi, G. Parisi, A. Sutera, and A. Vulpiani, Tellus **34**, 10 (1982).
[11] J. F. Lindner, M. Bennett, and K. Wiesenfeld, Phys. Rev. E **72**, 051911 (2005).
[12] H. Hu, K. Nakano, M. P. Cartmell, R. Zheng, and M. Ohori, J. Phys.: Conf. Ser. **382**, 012024 (2012).
[13] R. Zheng, K. Nakano, H. Hu, D. Su, and M. P. Cartmell, J. Sound Vib. **333**, 2568 (2014).
[14] H. A. Kramers, Physica **7**, 284 (1940).
[15] L. Gammaitoni, F. Marchesoni, and S. Santucci, Phys. Rev. Lett. **74**, 1052 (1995).
[16] See Supplemental Material at http://link.aps.org/supplemental/10.1103/PhysRevE.94.062205 for a MATHEMATICA notebook that checks the details of these calculations.
[17] To help concentrate the signal power in the drive bin of the discrete power spectrum, each Fourier-transformed time-series segment should contain an integer number of drive periods, if feasible. When using a radix-2 fast Fourier transform algorithm, each time-series segment should be a power-of-2 number of sample times.
[18] S. Michelin, S. G. L. Smith, and B. J. Glover, J. Fluid Mech. **617**, 1 (2008).
[19] Y. Xia, S. Michelin, and O. Doaré, Phys. Rev. Appl. **3**, 014009 (2015).
[20] J. F. Lindner, B. K. Meadows, W. L. Ditto, M. E. Inchiosa, and A. R. Bulsara, Phys. Rev. Lett. **75**, 3 (1995).
[21] J. F. Lindner, S. Chandramouli, A. R. Bulsara, M. Löcher, and W. L. Ditto, Phys. Rev. Lett. **81**, 5048 (1998).